

AperTO - Archivio Istituzionale Open Access dell'Università di Torino

Hematite nanoparticles larger than 90 nm show no sign of toxicity in terms of Lactate Dehydrogenase release, Nitric Oxide generation, apoptosis, and Comet Assay in Murine Alveolar Macrophages and Human Lung Epithelial Cells

This is the author's manuscript

Original Citation:

Availability:

This version is available <http://hdl.handle.net/2318/116147> since

Published version:

DOI:10.1021/tx2004294

Terms of use:

Open Access

Anyone can freely access the full text of works made available as "Open Access". Works made available under a Creative Commons license can be used according to the terms and conditions of said license. Use of all other works requires consent of the right holder (author or publisher) if not exempted from copyright protection by the applicable law.

(Article begins on next page)



UNIVERSITÀ DEGLI STUDI DI TORINO

This is an author version of the contribution published on:

Questa è la versione dell'autore dell'opera:

Freyria et al, J Chem. Res. Toxicol., Vol. 25 (4), 2012, pagg 850–861

The definitive version is available at:

La versione definitiva è disponibile alla URL:

<http://pubs.acs.org/journal/crtoec>

Hematite nanoparticles larger than 90 nm show no sign of toxicity in terms of lactate dehydrogenase release, nitric oxide generation, apoptosis and comet assay in murine alveolar macrophages and human lung epithelial cells.

Francesca Stefania Freyria,[†] Barbara Bonelli,^{†*} Maura Tomatis,^{‡*} Mara Ghiazza,[‡] Elena Gazzano,[§] Dario Ghigo,[§] Edoardo Garrone,[†] Bice Fubini.[‡]

[†]*Department of Applied Science and Technology, and INSTM-unit of Torino Politecnico, Politecnico di Torino, Corso Duca degli Abruzzi 24 Torino I-10129 (Italy)*

[‡]*Department of Chemistry IFM and “G. Scansetti” Interdepartmental Centre for Studies on Asbestos and other Toxic Particulates, Università degli Studi di Torino Via P. Giuria 7 Torino I-10125 (Italy).*

[§]*Department of Genetics, Biology and Biochemistry and “G. Scansetti” Interdepartmental Center for Studies on Asbestos and other Toxic Particulates, Università degli Studi di Torino Via Santena 5/bis Torino I-10126 (Italy).*

ABSTRACT

Three hematite samples were synthesised by precipitation from a FeCl₃ solution under controlled pH and temperature conditions in different morphology and dimensions: i) micro-sized (average diameter 1.2 µm); ii) sub-micro-sized (250 nm); iii) nano-sized (90 nm). To gain insight into reactions potentially occurring *in vivo* at the particle-lung interface following dust inhalation, several physico-chemical features relevant to pathogenicity were measured (free radical generation in cell-free tests, metal release, antioxidant depletion) and cellular toxicity assays on human lung epithelial cells (A549) and murine alveolar macrophages (MH-S) were carried out (LDH release, apoptosis detection, DNA damage, nitric oxide synthesis). The decrease in particles size – from 1.2 micron to 90 nm - only caused a slight increase in structural defects (disorder of the hematite phase and presence of surface ferrous ions) without enhancing surface reactivity or cellular responses in the concentration range between 20 and 100 µg/cm².

KEY-WORDS: hematite nanoparticles; sol-gel synthesis; free radicals generation; iron ions release; cytotoxicity, genotoxicity

1

¹ **NON-STANDARD ABBREVIATIONS.** CCD, Charge Coupled Device; BCA, bicinchoninic acid; LDH, lactate dehydrogenase; DAPI, 4',6-diamidino-2-phenylindole; NF-kb, nuclear transcription factor.

INTRODUCTION

Toxicological aspects of the chemistry of iron are of great interest for at least three reasons: i) iron is the most abundant transition element in nature and in the human body; ii) iron oxides, both micro- and nano-sized, are employed for various industrial applications^{1,2}; iii) iron ions may catalyze free radical generation in biological systems³⁻⁵ thus playing a key role in the toxicity of several mineral dusts⁶⁻⁸. Not all iron-containing minerals, however, are toxic⁹ nor always generate free radicals¹⁰: their generation depends on the redox potential and the coordination state of the iron ions at the solid surface and is not merely related to its content^{10,11}.

Hematite is the most abundant iron oxide polymorph. It is a key player in the geocycling of elements, rock weathering and soil formation^{12,13}, widely used in industry of fine ceramics, pigments, paints and catalysis¹⁴ and found in welding and in blast furnaces fumes^{15,16}. Hematite is also a component of the fly ash from solid waste incinerators^{17,18}. As a consequence airborne hematite particles were often found both in the occupational environment and in urban air^{19,20}, with median diameters ranging from several microns to few hundred nanometers¹².

Hematite in micrometric size exhibits a very low toxicity in cellular and cell-free tests, if any: it does not produce free radical species in cell-free systems¹⁰, is not cytotoxic, and does not induce neoplastic transformation in mouse embryo cells²¹, nor reactive oxygen species (ROS) generation in rabbit tracheal epithelial cells^{22,23}. Moreover, intrapulmonary instillation in humans produces only a transient inflammation²⁴.

A decrease in size, however, might cause toxicity, because, with crystalline dusts it usually increases the amount of structural defects and may consequently induce modifications of some properties responsible for toxicological effects^{25,26}. The extent of these defects depends on the nature and the size of particles and is more pronounced at the nanolevel²⁷.

As it concerns iron oxides, there are conflicting data on the effect of size on particle toxicity. Some *in vivo* studies showed that both nano- (22 nm) and submicron-sized (280 nm) Fe₂O₃ particles induce pulmonary injury²⁸ and neurotoxicity in rats²⁹, although to a different extent, while Karlsson

and coworkers³⁰ did not find clear differences between nano- (30 nm) and micro- (1 μm) particles in the ability to cause cell death, mitochondrial damage and oxidative DNA lesions in human lung epithelial cell line A549. Afterwards several studies on different cells types showed that Fe_2O_3 nanoparticles may induce oxidative stress^{31,32} and DNA breakage³², may reduce cell viability³² and may increase the nitric oxide levels³³. Such variability in cellular responses could be related to a different surface reactivity modulated by features like presence of contaminants, other polymorphs, surface defects etc.².

Aim of this work is to evaluate the effect of a decrease in size, from about 1 μm to about 100 nm, on some physico-chemical features considered relevant to pathogenicity and on some relevant cellular responses³⁴. For this purpose three hematite samples with controlled morphology having micro (average diameter 1.2 μm), sub-micro (250 nm), and nano-size (90 nm) were prepared.

Beside physico-chemical characterization of particles (Powders X-ray diffraction, Field Emission-Scanning Electron Microscopy, specific surface area determination, particles size distributions, Raman spectroscopy), the presence of Fe^{2+} ions at the surface, the amount of bio-available iron and the surface reactivity in the induction of oxidative stress were evaluated, respectively by mobilization with specific chelators and by checking both the ability to generate radical species (spin trapping) and to deplete some of the body antioxidant defences (incubation of the sample in a cysteine solution).

Finally, several evidences of both cytotoxicity and genotoxicity and the potential to generate reactive nitrogen species (RNS) have been investigated in both murine alveolar macrophages (MH-S) and in human lung epithelial cells (A549).

MATERIALS AND METHODS

Chemical reagents. When not otherwise specified, reagents were from Sigma-Aldrich S.r.l. (Milan, Italy).

Materials synthesis

The three α -Fe₂O₃ samples were prepared by a precipitation method based on the hydrolysis of iron (III) chloride (FeCl₃·6H₂O, ACS reagent 97%) in acidic solution prepared by diluting 37% w/w HCl (ACS reagent) with bi-distilled water (Carlo Erba). The following parameters, known to affect both morphology and dimensions of the particles, were carefully controlled during the synthesis: pH, Fe³⁺ ions concentration, temperature of hydrolysis and aging time³⁵. The three samples obtained with different average particles size will be hereafter referred to as Hem_nano, Hem_submicro and Hem_micro.

Hem_nano (average nanoparticles diameter of 90 nm) was prepared by dissolving FeCl₃·6H₂O into a 0.002 M HCl aqueous solution preheated at 98 °C, until the final concentration of Fe³⁺ ions was 0.02 M. The solution was then stirred at 200 rpm for about 30 min, by maintaining the temperature in the 95-100°C range and adjusting the pH at about 2.3.

Hem_submicro (average nanoparticles diameter of 250 nm) was obtained by diluting a 0.5 M Fe³⁺ solution with a 0.025 M HCl solution at room temperature and pH around 1.1.

Hem_micro (average particles diameter of 1.2 μm) was synthesized by hydrolysis of a 0.1 M Fe³⁺ solution in 0.05 M HCl solution at 95 °C (30).

The solutions thus prepared were then transferred to a Teflon autoclave, sealed and left to stand in oven at either 100 °C (Hem_nano and Hem_submicro samples) or 120 °C (Hem_micro sample), for one week in static conditions. Precipitates were recovered by centrifuging (ALC centrifuge PK110, 4000 rpm for 90 min) and washing the resulting suspensions with bi-distilled water, until clear supernatant liquids were obtained. Powders were then dried and stored at room temperature.

Crystallographic and morphological characterization

Powders X-ray diffraction (XRD) patterns were collected on a X'Pert diffractometer (Phillips) using Cu K_α radiation (1.541874 Å) (scan range 10° - 90° 2θ, step width 0.02°). All

diffraction patterns were indexed by using the PDF-2 Release 2002 database. Average crystallites size was calculated from XRD patterns according to Scherrer equation (Table 1).

Field Emission-Scanning Electron Microscopy (FE-SEM) pictures were collected on a High Resolution instrument (LEO 1525) equipped with a Gemini Field Emission Column; Transmission Electron Microscopy (TEM) pictures were collected on a Philips CM12 TEM instrument, operating at 120 kV (LaB₆ filament, equipped with a 622 SC CDD YAG Gatan). Average particles size were measured by means of the Image J software on both FE-SEM and TEM images, by analyzing 3-5 micrographs for each sample (Table 1).

The Specific Surface Area (SSA) of the samples was measured by using the BET (Brunauer – Emmett – Teller) method by means of N₂ sorption isotherms at -196°C on powders pre-outgassed at 150°C for about 4-6 h in order to remove water and other atmospheric contaminants (Quantachrome Instruments Autosorb 1C). Values of geometrical area were also calculated from the relationship $6/\rho d$, where ρ is hematite density (5.26 g cm⁻³), d the average diameter (or side) of particles assumed with either spherical or pseudo-cubic shape as determined by FE-SEM.

Particles size distribution (PSD) was measured by means of Dynamic Light Scattering (DLS) on diluted suspensions of samples dispersed in the same biologic medium used for cellular toxicity assay (*vide infra*) (Zetasizer Nanoseries ZS90, Malvern instrument, for accurate measurement of particles dimensions in the 2-3000 nm range).

Micro-Raman spectra were acquired using an integrated micro/macro Raman system Jobin Yvon Mod. The system includes a Horiba Jobin Yvon HR800 microspectrometer, an Olympus BX41 microscope and a CCD air-cooled detector. A polarized solid state Nd laser operating at 532 nm was used as the excitation source. Calibration was checked by measuring the Stokes and anti-Stokes bands of the Si band at ± 520.7 cm⁻¹. Each spectrum was acquired using a 100X microscope objective. In order to produce strong signals without inducing surface alteration due to heat, the laser beam was focused to a spot size of 2 μ m and a filter with optical density $d=0.6$ was inserted (laser power 0.35 mW). To optimize the signal to noise ratio, spectra were acquired using 5 scans of

10 seconds for each spectral region. The curve-fitting was carried out by OPUS program and was based on the damped least-squares optimization algorithm developed by Levenberg–Marquardt. The curve-fitting procedure was applied in the region between 1700 and 900 cm^{-1} .

Evaluation of surface defectivity

The amount of Fe^{2+} ions at the surface of the samples was evaluated by removal by a bidentate N donor chelator specific for Fe^{2+} ions. Hematite particles (1 mg ml^{-1}) were suspended (up to a final volume of 100 ml) in a 0.15 M NaCl solution containing 1 mM ferrozine at $\text{pH} = 4.5$ for 5 days at $37\text{ }^\circ\text{C}$ and continuously shaken. The Fe^{2+} -ferrozine complex was determined by measuring the absorbance at 562 nm ($\epsilon_{\text{mM}} = 27.9\text{ mM}^{-1}\text{ cm}^{-1}$) on an Uvikon 930 dual beam spectrophotometer (Kontron Instrument). The data are expressed per unit surface area and reported as mean \pm SD (Standard Deviation) of two distinct experiments.

Surface reactivity related to oxidative stress

Bioavailable iron: the amount of iron (Fe^{3+} and Fe^{2+}) released from the hematite surface was measured following incubation (1 mg ml^{-1}) in a solution 1 mM of ferrozine containing ascorbic acid (1mM), using the same protocol described above for determination of the surface defects. Ascorbic acid was used to reduce Fe^{3+} to Fe^{2+} to measure the total amount of Fe mobilized³⁶. The data are expressed per unit surface area and reported as mean \pm SD of two distinct experiments.

Free radical release. The radical release upon incubation of hematite, with either H_2O_2 (yielding hydroxyl radicals) or sodium formate (yielding carbon centred radicals following homolytic cleavage of C-H bonds) was detected using the spin trapping technique with 5,5'-dimethyl-1-pyrroline-N-oxide (DMPO) as trapping agent. The production of HO^\bullet radicals was measured by suspending 25 mg sample in 500 μl of 0.5 M phosphate buffer ($\text{pH} = 7.4$), then adding

250 μl of 0.17 M DMPO and 500 μl of 0.2 M H_2O_2 . The production of $\text{CO}_2^{\cdot-}$ radicals was measured by suspending 25 mg sample in 500 μl of 0.17 M DMPO, then adding 500 μl of a 2 M sodium formate solution in 0.5 M phosphate buffer. The generation of carbon centered radicals was tested also in the presence of ascorbic acid (1.5 mM) as reducing agent. The radical adducts formed were monitored by Electron Paramagnetic Resonance (EPR) spectroscopy. The number of radicals released is proportional to the intensity of the EPR signal measured by double integration. Kinetics of free radical yield was followed for at least 1 h¹⁰.

Cysteine consumption. The reaction of cysteine with the hematite samples was measured by incubating 100 mg powder with 10 mL of a 0.10 mM cysteine solution in phosphate buffer (pH=7.4). The suspension was stirred at 37°C for 3 h. At regular time intervals, the suspension was centrifuged (6000 rpm, 10 minutes) and filtered on mixed cellulose esters membrane (Millipore, pore diameter =0.05 μm). The amount of cysteine in solution was measured spectrophotometrically (Uvikon 930) at 412 nm by Ellman's reagent³⁶. The data are reported as mean \pm SD of two distinct experiments.

Cellular toxicity assay

Cells. Human lung epithelial cells (A549) and murine alveolar macrophages (MH-S), provided by Istituto Zooprofilattico Sperimentale "Bruno Ubertini" (Brescia, Italy), were cultured in 35 mm-diameter Petri dishes in RPMI-1640 (Gibco, Paisley, UK) supplemented with 10% FBS up to 90% confluence, and then incubated in the same culture medium for 24 h in the absence or presence of particles before the assays. The protein content of the cell monolayer was assessed with the BCA kit. Before the incubation the particles were dispersed in the culture medium and sonicated twice for 2 min on ice (Labsonic sonicator, 100 W) to allow a better suspension and diffusion. For cellular

tests Min-U-Sil 5 crystalline quartz (US Silica Company, Berkeley Springs, WV), the most widely employed silica sample *in vitro* and *in vivo* studies, was used as a positive control.

Cytotoxicity. The cytotoxic effect of the hematite particles was measured as leakage of LDH activity from the cell into the extracellular medium, as previously described³⁷. Briefly, after a 24 h incubation, the extracellular medium was collected and centrifuged at 13,000 x g for 60 min. The cells were washed with fresh medium, detached with trypsin/EDTA (0.05/0.02% v/v), washed with PBS, re-suspended in 1 ml of TRAP solution (triethanolamine 82.3 mM, pH = 7.6), and sonicated on ice with two 10-s bursts. LDH activity was measured both in the extracellular medium and in the cell lysate. The reaction was followed for 10 min, by measuring the absorbance at 340 nm (T = 37°C) with a Synergy HT microplate reader (Bio-Tek Instruments, Winooski, VT). Each kinetic reaction was linear throughout the time of measurement. Both intracellular and extracellular enzyme activities were expressed as μmol of NADH oxidized/min/dish, then extracellular LDH activity (LDH out) was calculated as percentage of the total (intracellular + extracellular) LDH activity (LDH tot) in the dish. The absence of interference of the particles with LDH assay was verified by mixing the samples with the reaction mix: the particles did not induce any variation in absorbance (340 nm) measurement (data not shown).

Nitric oxide (NO) synthesis. After 24 h incubation in the absence or presence of hematite particles, the culture supernatant was removed, centrifuged at 13,000 x g for 60 min and tested for nitrite, which is a stable derivative of NO, using the Griess method as previously described³⁸. The amount of nitrite was corrected for the content of cell proteins, measured with the BCA kit, and results were expressed as nmol/mg cellular protein. Appropriate controls (*i.e.* cell-free suspensions) have been included to exclude any interference of the particles with this colorimetric assay (data not shown).

Alkaline Comet Assay. Single-cell gel electrophoresis (comet assay) was performed under alkaline conditions according to the method of Singh et al.³⁹ with slight modifications. All steps were conducted under dim yellow light to prevent additional DNA damage. A 7.5 μl cell suspension

(5×10^4 cells) was mixed with 75 μ l of low melting point agarose (0.8%) and placed on the clear part of a frosted microscope slide pre-coated with a layer of normal melt point agarose (1%) and low melting point agarose. Then, slides were immersed in lysis buffer for 1 h (4 °C, 2.5 M NaCl, 0.1 M Na₂EDTA, 10 mM Tris, 0.5% N-laurylsarcosine, supplemented with 1% Triton X-100 just before use). To perform the DNA unwinding, slides were placed in a horizontal electrophoresis unit containing the electrophoresis buffer (300 mM NaOH, 1 mM Na₂EDTA, pH > 13) for 40 min. Alkaline electrophoresis was performed in the same buffer for 20 min (25 V, 300 mA). Slides were washed three times with neutralization buffer (0.4 M Tris, pH 7.5), and then they were dehydrated in 70% ethanol (5 min) and left to dry, allowing storage until analysis. To analyze DNA damage, slides were stained with DAPI (10 μ g ml⁻¹, 5 min). Fifty randomly chosen, non-overlapping comets per comet slide were observed using a Leica fluorescence microscope (20X objective) and an image analysis system (CometScore, TriTek Corp., Sumerduck, VA).

Detection of Apoptosis. The induction of apoptosis or necrosis was performed as previously described³⁷. After a 24 h incubation in the absence or presence of particles, the cells were washed with PBS, detached with trypsin/EDTA, added to floating cells previously collected from the supernatant, and resuspended at 3×10^5 cells/0.5 ml of binding buffer [containing 10 mM N-(2-hydroxyethyl)piperazine-N'-ethanesulfonic acid (Hepes), 2.5 mM CaCl₂, and 140 mM NaCl, pH 7.4]. These cell suspensions were incubated for 10 min with 25 μ g of propidium iodide (PI, Calbiochem-Novabiochem Corp., La Jolla, CA) and 5 μ l of annexin V-fluorescein isothiocyanate (FITC) (0.05 mg ml⁻¹). Cells were washed, and fluorescence was measured at 488 (excitation)-530 nm (emission) for annexin V or 536 (excitation)-617 nm (emission) for PI detection using a Synergy HT microplate reader. Results were expressed as average percentage values obtained from triplicate experiments versus controls.

Statistical analysis. All data from cellular tests in the following text and figures are provided as means \pm SEM (standard error of mean). The results were analyzed by a one-way Analysis of

Variance (ANOVA) and Tukey's test (software: SPSS 11.0 for Windows, SPSS Inc., Chicago, IL). $p < 0.05$ was considered significant.

RESULTS

Crystallographic and morphological characterization

XRD patterns of the three powder samples, reported in Figure 1, only showed the peaks of rhombohedral hematite (α -Fe₂O₃): a pure phase was obtained, within the limits of XRD technique that cannot detect any phase when present in *ca.* less than 5% weight. The average crystallite size was calculated, from XRD patterns, according to the Scherrer equation: the crystallite size of Hem_nano and Hem_submicro samples was close to the average particle size as measured by either FE-SEM or TEM images (Table 1), whereas a discrepancy was observed with Hem_micro sample, probably due to the occurrence of polycrystalline particles in the latter.

The particle morphology is illustrated in the FE-SEM and TEM pictures reported in Figures 2 and 3. Hem_nano particles were rather spherical and homogenous in size (Figure 2a), whereas with increasing particle dimension, the shape approached the one of α -Fe₂O₃ “perfect” rhombohedra. Indeed Hem_submicro particles became more heterogeneous in both shape and size (Figure 2b), did not show any longer the spherical shape of smaller particles, with even particles larger than 250 nm observed. Hem_micro sample (Figure 2c) only exhibited micrometric rhombohedral particles. The TEM pictures (Figure 3) confirmed the morphological features observed by FE-SEM for Hem_nano and Hem_submicro particles: the most interesting result was, however, the confirmation that Hem_micro particles are polycrystalline (Figure 3c). Selected area electron diffraction (SAED) patterns reported in the inset showed concentric and unfocused spots indicating the presence of overlapping crystals. Their polycrystalline nature may explain the different values of both Scherrer diameter and average particle size. The magnification reported in

Figure 3d shows that the elongated dimension of those sub-crystals measured in the micrograph was close to the Scherrer diameter derived by the XRD patterns (Table 1).

BET SSA values, as obtained by measurements on different sample batches, are reported in Table 1: the one of Hem_nano was in the 19-22 m² g⁻¹ range, the small spread, of obtained values indicating that the sample is homogeneous, as shown by FE-SEM. Hem_submicro value is lower (4-8 m² g⁻¹) the observed variability being in agreement with its morphological heterogeneity evidenced by FE-SEM analysis. Finally, Hem_micro exhibited a higher surface area (14 m² g⁻¹) than what expected on the mere basis of the particle morphology.

In order to evaluate the possible contribution of surface defect, roughness *etc.* to the actual (measured) SSA of the samples, the BET values were compared to the geometrical (theoretical) areas reported in Table 1. In all cases, the measured SSA are larger than the geometrical areas, the most evident mismatch being observed for the Hem_micro sample.

To evaluate the tendency to form aggregates, the size distribution of the hematite samples suspended in the medium used for cellular tests was evaluated by DLS.

Figure 4 reports the results of PSDs analysis on the three samples under study. For each samples, three curves are reported corresponding to the actual experimental curve (intensity) and to percentages by volume and number, the latter two representations allowing to evaluate particle size homogeneity. The corresponding values of particles hydrodynamic diameter (PHD), Poly-Dispersion Index (PDI) and mean are gathered in Table 2. With Hem_nano, PSDs curves in volume and number were rather narrow and overlapped (Figure 4a), confirming that hematite nanoparticles with homogenous size distribution occur also after suspending the sample in the biological medium. Hem_micro sample had very symmetric and narrow PSD curves (Figure 4c), with a PHD of 762 nm. The latter result must, however, be considered with care, since FE-SEM pictures showed that larger rhombohedral particles were obtained, and could be due to some particles deagglomeration occurring in biologic medium and/or to the different methods of measurement adopted by the two techniques. With Hem_submicro sample, less homogeneous PSD curves were observed (Figure 4b),

with different shapes, not overlapped, and with a peak corresponding to the presence of larger particles in the PSD curve by volume. Such a result was in agreement with FE-SEM analysis of the powder sample (Figure 2b), showing heterogeneous particles in both size and shape. The values of Poly-Dispersion Index reported in Table 2 were below 0.5 and should be an indication of monomodal PSDs, besides the presence of some aggregates/agglomerates.

Figure 5a shows the Raman spectra of the samples in the 150 -1800 cm^{-1} range. All spectra exhibited the typical features for $\alpha\text{-Fe}_2\text{O}_3$ crystals. The main features were six peaks at about 226 (A_{1g}), 245 (E_g), 298 (E_g), 412 (E_g), 500 (A_{1g}) and 612 (E_g) cm^{-1} , which are due to the symmetry-allowed modes indicated in parentheses, and two extra peaks at about 660 cm^{-1} and 1320 cm^{-1} . The band at 1320 cm^{-1} is due to an overtone. The peak at 660 cm^{-1} is known as the low order (LO) band and is likely to be due to the Raman forbidden E_u mode that becomes activated through disorder-induced breaking of the symmetry properties by scattering the LO phonon. The LO band usually decreases in intensity with increasing particle sizes⁴⁰.

Defectivity evaluation was performed by comparing the 612 cm^{-1} (E_g) and 660 cm^{-1} (LO) bands. E_g /LO intensity ratios for the three samples were: Hem_micro 0.7 ± 0.1 , Hem_submicro 1.6 ± 0.3 and Hem_nano 0.9 ± 0.2 . As expected, Hem_nano exhibited a lower E_g /LO intensity ratio than Hem_submicro. This indicates a more ordered structure in the fine particles than in the ultrafine ones. Conversely, E_g /LO for the micrometric sample was quite similar to the E_g /LO for the nanometric one.

Evaluation of surface defectivity

Figure 6 shows the amount of ferrous ion released per unit surface area during 5 days of incubation. All hematite samples released Fe^{+2} in solution, but in very small amounts. At the end of incubation, the amount of Fe^{+2} released ranged between 0.1 and 0.3 $\mu\text{mol m}^{-2}$. All samples were able to release Fe^{+2} after a short time of incubation, indicating the presence of highly uncoordinated

ions, *e.g.* ions most probably located at edge or corner positions, and therefore prone to be removed. Hem_nano released a higher amount of ferrous ions, revealing a larger surface defectivity if compared to Hem_submicro and Hem_micro particles.

Surface reactivity related to oxidative stress

Bioavailable iron: Figure 7 shows the amount of total iron released (both Fe³⁺ and Fe²⁺) as a function of time. Iron ions were mobilized from all samples. No significant differences were found between Hem_nano and Hem_submicro. After 24 h of incubation the amount of iron released was 2.8 $\mu\text{mol m}^{-2}$ and slowly increased over time up to of 3.2 $\mu\text{mol m}^{-2}$ after 72 h. Interestingly, the amount of iron released by the micrometric sample was lower in the first period of incubation. After 24 h iron mobilized was about 2 $\mu\text{mol m}^{-2}$ and progressively increased approaching, after 7 days, the iron released by the Hem nano and Hem-submicro samples.

Free radical generation: Two radical-generating mechanisms have been investigated, by means of the spin trapping technique: i) production of HO[•] species in the presence of H₂O₂, mimicking contact of the particles with hydrogen peroxide produced by cell-generated superoxide anion; ii) production CO₂^{•-} species from the formate ion, used as a model target molecule for a homolytic cleavage of a carbon-hydrogen bond.

In agreement with former studies¹⁰, Hem_micro particles produced neither hydroxyl radical nor carbon centred radicals. The reduction in size did not involve the ability to generate free radicals, in spite of the presence of some Fe²⁺. The addition to the reaction medium of ascorbic acid, an endogenous reducing agent, did not generate surface sites active in free radical release (results not reported for brevity).

Cysteine consumption: The amount of cysteine consumed after both 30 min and 180 min of incubation with a 0.1 mM solution is shown in Table 3. After 30 min of incubation, all hematite samples consumed cysteine at a similar extent, few differences among the different hematite

appeared only after 180 min of incubation. Hem_nano sample was just slightly less reactive than Hem_micro and Hem_sub-micro.

Cellular toxicity assays

After a 24 h incubation hematite particles at the concentrations of 20-40-80-100 $\mu\text{g cm}^{-2}$ did not induce, in MH-S cells, a significant cytotoxic effect, measured as leakage of intracellular LDH activity into the extracellular medium (Figure 8). Hematite particles did not increase LDH release also in human lung epithelial A549 cells (Figure S1, Supporting Information).

To determine whether the exposure to hematite particles resulted in apoptotic death, after a 24 h incubation we stained MH-S cells with annexin V-FITC and PI. The positive control significantly increased the amount of both annexin V-FITC-positive (an index of apoptosis) and PI-positive cells (an index of necrosis), already at 20 $\mu\text{g cm}^{-2}$, and this effect increased further at higher concentrations (Figure 9). These data suggest that, after a 24 h incubation with the positive control, the majority of damaged MH-S cells was in late apoptosis or necrosis. On the contrary, neither apoptosis nor necrosis was observed when cells were incubated with hematite particles, at all the concentrations tested. Similarly, in A549 cells hematite particles did not induce apoptosis nor necrosis, even at 100 $\mu\text{g cm}^{-2}$ (Figure S2, Supporting Information).

After a 24 h incubation in the absence or presence of hematite particles, MH-S cells were subjected to single-cell gel electrophoresis (comet assay) (Figure 10). Tail DNA (percentage of DNA in the tail), an index of DNA damage, was not modified following incubation with 40 $\mu\text{g cm}^{-2}$ of hematite particles (Figure 10), while it was significantly higher in MH-S cells incubated with 20 $\mu\text{g cm}^{-2}$ of the positive control in comparison with cells in the absence of particles. A lower concentration was used for the positive control, because at 40 $\mu\text{g cm}^{-2}$ it induced excessive cytotoxicity. Similarly, hematite particles did not induce genotoxicity in A549 cells (Figure S3, Supporting Information).

The extracellular level of nitrite was measured in MH-S cells after a 24 h incubation with particles. None of the hematite particles induced a significant increase in nitrite production at any of the concentrations tested (Figure 11). No effect was actually detected in A549 cells: hematite particles did not increase NO production (Figure S4, Supporting Information).

In the Supporting Information we have also reported all data normalized per unit of exposed surface area: in all the experiments performed (LDH leakage, apoptosis induction, DNA damage and NO production) and in both cell lines, hematite nanoparticles were inactive.

DISCUSSION

Bulk composition

Both XRD and Raman analysis showed that a pure hematite phase was obtained with the three samples, whatever their size. Besides hematite bands, Raman spectra also revealed the presence on all samples of a band at about 660 cm^{-1} , considered to be a signature of lattice disorder. The intensity of such band was higher with Hem_nano than with Hem_submicro, indicating a more disordered structure with the smaller-sized sample. Reduction in size, in fact, can affect stoichiometry and structure of both crystal interior and surface, creating discontinuous crystal planes⁴⁰. In contrast, the extent of lattice disorder, as measured by Raman spectroscopy, in Hem_micro was similar to the one of Hem_nano sample, the latter result being in agreement with the stepped crystalline structure of Hem_micro particles, observed in TEM pictures (Figures 3c and 3d).

Surface composition and reactivity related to oxidative stress

Oxygen-defectivity, with consequent occurrence of ferrous ions, is often observed at the surface of hematite⁴¹. As a whole, a small amount of Fe^{2+} ions was observed with the three hematite samples studied, in a size-dependent extent, because the amount of ferrous ions detected slightly decreases with increasing the particle size. The surface sites containing Fe^{2+} could act as catalytic centres for free radical generation^{10,42,43}. Moreover, Fe^{2+} could be released in solution when in

contact with biological fluid. Iron mobilization is of great interest in particle toxicology because iron in solution may play a crucial role in several biochemical reactions e.g. DNA damage⁴⁴ and in several cellular effect^{6,45}. Lay²⁴ hypothesized that the transient inflammation observed in human lung after instillation of micro hematite was due to soluble iron. Similarly, some studies show that iron dissolution is responsible for cytotoxicity induced by hematite nanoparticles in mesothelial cells⁴⁶, for oxidative stress in endothelial cells³³ and for HO[•] radical release in cell-free tests⁴⁷ elicited by both Fe₃O₄ and Fe₂O₃ nanoparticles, although in the latter case iron in solution was less reactive than surface sites.

The leaching of iron (both in reduced and oxidized form) from an iron oxide may be the result of dissolution at the acidic pH, e.g in the lysosomes⁴⁸, or of chelation by endogenous molecules⁴⁹. The bioavailable iron was determined here by incubation of hematite in a solution at acidic pH containing a specific Fe²⁺ chelator and ascorbic acid in order to reduce Fe³⁺ to Fe²⁺. Fe²⁺ is released into the solution much faster than Fe³⁺, because the bonds between the reduced iron and O²⁻ ions of the crystalline lattice are weakened.

As expected, only small amounts of iron ions were mobilized during one week of incubation. Hematite in fact is a stable oxide with iron ions well coordinated at the surface. At the end of the incubation the iron released was 3-5 times less than the iron extracted, under similar test conditions, from other iron-rich minerals such as asbestos^{36,50} and basaltic volcanic ash⁸. Similar amounts of iron were mobilized from Hem_nano and Hem_submicro, while, as expected, the micrometric sample showed a lower solubility⁵¹. However after some days of incubation the iron released by Hem_micro approached the other two samples. This could be related to the polycrystalline nature of this sample with edge and kinks at the surface, which facilitate iron extraction.

Free radical release by inorganic dusts and their potential to interact with endogenous molecules involved in the antioxidant defences are among the surface properties most relevant to

toxicity⁵². The potential of hematite to generate radical species in solution at physiological pH and to induce a depletion of cysteine have thus been compared.

HO[•] generation may be induced through the reaction of Fe²⁺ with H₂O₂. This reaction, referred to as Fenton reaction, may occur through Fe²⁺ present on the particle surface or released into solution.



However, also materials only containing Fe³⁺ at the surface may release HO[•] radicals through a Fenton-like reaction, that requires previous reduction of Fe³⁺ to Fe²⁺ by endogenous molecules such as ascorbic acid (iron-catalyzed Haber–Weiss reaction) or by reaction of Fe³⁺ and H₂O₂ with HO₂[•] formation as propagating intermediate⁵³. Despite a number of studies on the different iron-rich toxic particulates, the nature of surface iron sites involved in the Fenton and Fenton-like reactions is not yet completely clear. It is noteworthy that such ions have to be accessible and in a specific coordination state¹¹. As shown above, both Fe²⁺ and Fe³⁺ ions in low coordination state (thus prone to be removed) were present at the particle surface, even if their amount is small if compared to other minerals highly active in radical generation^{8,36,50}. However, despite the small differences in the abundance of iron ions, none of the three hematite samples was able to generate radical species. Note that the total amount of iron released was for all samples 5 times less than the one released by a micrometric sample of hematite, which has been found responsible for the acute pulmonary inflammation in humans²⁴.

Similarly no great differences on the basis of particles size may be observed in antioxidant depletion. The respiratory tract lining fluid is the first physical defence encountered by inhaled particles entering the respiratory system and is known to contain antioxidants such as ascorbate and glutathione. The potential of particles to interfere with such defences is often evaluated by monitoring the depletion of antioxidants during incubation of the sample with endogenous molecules over time⁵⁴⁻⁵⁷. Cysteine was chosen since it is a precursor in the biosynthesis of reduced glutathione, and thus plays an important role in the intracellular and extracellular antioxidant

defences. Hem_micro was not very effective in the depletion of cysteine. The amount of cysteine consumed was 10-50 times less than the one consumed by other toxic particulates, such as asbestos³⁶ or quartz⁵⁷. The size decrease only induced a small increase in the consumption. Cysteine depletion may occur through different mechanisms such as oxidation of the thiol group⁵⁷, or adsorption on the solid surface mainly via complex formation with surface Fe⁺³ and subsequent iron oxide dissolution⁴⁹. Since no radical activity was detected, the reductive dissolution governed by formation of complex with Fe³⁺ is more likely.

Cellular toxicity

Nitrite is the stable derivative of NO, which is produced by three NO synthase (NOS) isoforms and plays many important roles, including unspecific immune response, being effective against various microbes and tumour cells. During a chronic inflammatory reaction, however, elevated NO tissue levels can be toxic also for host cells. NO can react with the superoxide anion, producing either peroxynitrite, which in turn can generate hydroxyl radicals, and reactive nitrogen species able to interact with proteins and nucleic acids⁵⁸. Some iron oxides, mainly in nano-size, are able to increase the iNOS activity^{33,59}. Other toxic particulates are able to activate iNOS. Iron-rich minerals (e.g. crocidolite asbestos) are able to increase NO levels in rat lung epithelial and mesothelial cells⁶⁰. It has been suggested that, in human lung epithelial cells, iron released from asbestos induces oxidative stress, associated with the iron-independent decrease of intracellular glutathione; these events could activate NF-kB, thus inducing iNOS expression⁶¹. Similarly, some crystalline silica are able to induce iNOS activation^{62,63}. In the present work no alteration in the iNOS activity was observed in macrophages neither in human epithelial cells. The inactivity of all hematite samples may thus be related both to the low surface reactivity in radical generation and to the low ability to release iron ions in solution. No signs of cytotoxicity were observed in apparent contrast with past studies demonstrating a reduction of viability in several cell types incubated with

hematite nanoparticles, although in a different extent^{31,33,46,64,65}. The minimum dose required to observe a cytotoxic effect, in fact, ranged between 40 and 350 $\mu\text{g}/\text{cm}^2$ depending upon cell models, likely because of the different cell sensitivity. The cytotoxicity was related to iron release in solution⁴⁶ or to induction of oxidative stress via antioxidant enzyme consumption⁶⁴ or to free radical generation³². The low surface reactivity of the three hematite samples used in the present study may thus account for the observed lack of cytotoxicity.

In the present study, hematite nanoparticles did not induce DNA damage, measured with comet assay. Genotoxicity of hematite nanoparticles has been assessed in very few studies, with contrasting results depending on the conditions. No signs of DNA damage have been observed in A549 cells after a 4 h exposure to 20 and 40 $\mu\text{g}/\text{cm}^2$ nanoparticles⁶⁶, while a 24 h incubation with 10 and 50 $\mu\text{g}/\text{cm}^2$ nanoparticles was able to induce DNA breakage (measured with comet assay) respectively in human lung fibroblasts and human bronchial epithelial cells³². Oxidative DNA lesions were not observed following hematite nanoparticles exposure^{32,66}.

CONCLUSIONS

Results here reported confirm that hematite is a poorly reactive, non toxic material. The decrease in particles size from 1-2 μm to 80-100 nm only caused a slight increase of the structural defects (low ordering of the hematite phase and presence of surface ferrous iron ions). Such increase, however, did not enhance surface reactivity related to oxidative stress (free radical generation and depletion of cysteine). All hematite particles were non cytotoxic, did not induce apoptosis, did not stimulate RNS generation (yielding NO) and did not induce DNA damage, when incubated with human lung epithelial cells and murine alveolar macrophages. The absence of adverse cellular effects following size reduction suggests that nano-size alone when not associated to a specific surface reactivity should not be responsible for some adverse cellular responses.

The results of this study indicate that the size reduction from micrometric to submicrometric range, if not associated with a specific surface reactivity, does affect neither several aspects of

cytotoxicity and genotoxicity nor the potential to induce oxidative stress almost in human epithelial cells and murine alveolar macrophages. The differences in the surface reactivity may explain the differences in cellular responses observed by several authors in presence of iron oxides.

FUNDING

This research was carried out with the financial support of Regione Piemonte, project NANOSAFE “Nanoparticles: from their impact on the environment and human health to safer production and usage” (program CIPE 2006). The micro-Raman spectra were obtained with the equipment acquired by the “G. Scansetti” Interdepartmental Centre for Studies on Asbestos and Other Toxic Particulates, with a grant from Compagnia di San Paolo, Torino, Italy.

ACKNOWLEDGEMENTS

Prof. D.L. Marchisio (Politecnico di Torino) and Prof. E. Belluso (Università di Torino) are acknowledged for DLS measurements and TEM analysis, respectively. FE-SEM analysis was carried out at Agrifood Innovation Centre Tecnogranda (Dronero, CN, Italy).

SUPPORTING INFORMATION

Experiments performed on A549 cells (Figures S1, S2, S3, and S4). MH-S results normalized per unit of exposed surface area (Figures S5, S6, S7, and S8). This material is available free of charge via the Internet at <http://pubs.acs.org>.

REFERENCES

- (1) Corot, C., Robert, P., Idee, J. M., and Port, M. (2006) Recent advances in iron oxide nanocrystal technology for medical imaging. *Adv Drug Deliv Rev* 58, 1471-1504.
- (2) Huber, D. L. (2005) Synthesis, properties, and applications of iron nanoparticles. *Small* 1, 482-501.
- (3) Halliwell, B., and Gutteridge, J. M. (1990) Role of free radicals and catalytic metal ions in human disease: an overview. *Methods Enzymol.* 186, 1-85.
- (4) Pierre, J. L., and Fontecave, M. (1999) Iron and activated oxygen species in biology: the basic chemistry. *Biometals* 12, 195-199.
- (5) Pierre, J. L., Fontecave, M., and Crichton, R. R. (2002) Chemistry for an essential biological process: the reduction of ferric iron. *Biometals* 15, 341-346.
- (6) Aust, A. E., Lund, L. G., Chao, C. C., Park, S. H., and Fang, R. H. (2000) Role of iron in the cellular effects of asbestos. *Inhalation Toxicology* 12, 75-80.
- (7) Shafer, M. M., Perkins, D. A., Antkiewicz, D. S., Stone, E. A., Quraishi, T. A., and Schauer, J. J. (2010) Reactive oxygen species activity and chemical speciation of size-fractionated atmospheric particulate matter from Lahore, Pakistan: an important role for transition metals. *J Environ Monit.* 12, 704-715.
- (8) Horwell, C. J., Fenoglio, I., and Fubini, B. (2007) Iron-induced hydroxyl radical generation from basaltic volcanic ash. *Earth and Planetary Science Letters* 261, 662-669.

- (9) Steinhoff, D., Mohr, U., and Hahnemann, S. (1991) Carcinogenesis studies with iron oxides. *Exp. Pathol.* 43, 189-194.
- (10) Fubini, B., Mollo, L., and Giamello, E. (1995) Free radical generation at the solid/liquid interface in iron containing minerals. *Free Radic Res* 23, 593-614.
- (11) Turci, F., Tomatis, M., Lesci, I. G., Roveri, N., and Fubini, B. (2011) The iron-related molecular toxicity mechanism of synthetic asbestos nanofibres: a model study for high-aspect-ratio nanoparticles. *Chemistry-A European Journal* 17, 350-358.
- (12) Kandler, K., Schutz, L., Deutscher, C., Ebert, M., Hofmann, H., Jackel, S., Jaenicke, R., Knippertz, P., Lieke, K., Massling, A., Petzold, A., Schladitz, A., Weinzierl, B., Wiedensohler, A., Zorn, S., and Weinbruch, S. (2009) Size distribution, mass concentration, chemical and mineralogical composition and derived optical parameters of the boundary layer aerosol at Tinfou, Morocco, during SAMUM 2006. *Tellus Series B-Chemical and Physical Meteorology* 61, 32-50.
- (13) Arimoto, R., Balsam, W., and Schloesslin, C. (2002) Visible spectroscopy of aerosol particles collected on filters: iron-oxide minerals. *Atmospheric Environment* 36, 89-96.
- (14) Cornell RM, S. U. *The Iron Oxide: Structure, Properties, Reactions and Uses* (1996) Weinheim, VCH.
- (15) Koponen, M., Gustafsson, T., Kalliomaki, K., Kalliomaki, P. L., Moilanen, M., and Pyy, L. (1980) Dusts in a steel-making plant. Lung contamination among iron workers. *Int Arch Occup Environ Health* 47, 35-45.

- (16) Worobiec, A., Stefaniak, E. A., Kiro, S., Oprya, M., Bekshaev, A., Spolnik, Z., Potgieter-Vermaak, S. S., Ennan, A., and Van Grieken, R. (2007) Comprehensive microanalytical study of welding aerosols with x-ray and Raman based methods. *X-Ray Spectrometry* 36, 328-335.
- (17) Meima, J. A., and Comans, R. N. J. (1997) Geochemical modeling of weathering reactions in municipal solid waste incinerator bottom ash. *Environmental Science & Technology* 31, 1269-1276.
- (18) Fermo, P., Cariati, F., Pozzi, A., Demartin, F., Tettamanti, M., Collina, E., Lasagni, M., Pitea, D., Puglisi, O., and Russo, U. (1999) The analytical characterization of municipal solid waste incinerator fly ash: methods and preliminary results. *Fresenius Journal of Analytical Chemistry* 365, 666-673.
- (19) Ledoux, F., Zhilinskaya, E. A., Courcot, D., Aboukais, A., and Puskaric, E. (2004) EPR investigation of iron in size segregated atmospheric aerosols collected at Dunkerque, Northern France. *Atmospheric Environment* 38, 1201-1210.
- (20) Gomez, M. R. (1997) Factors associated with exposure in occupational safety and health administration data. *American Industrial Hygiene Association Journal* 58, 186-195.
- (21) Saffiotti, U., and Ahmed, N. (1995) Neoplastic transformation by quartz in the BALB/3T3/A31-1-1 cell line and the effects of associated minerals. *Teratog. Carcinog. Mutagen.* 15, 339-356.
- (22) Guilianelli, C., Baeza-Squiban, A., Boisvieux-Ulrich, E., Houcine, O., Zalma, R., Guennou, C., Pezerat, H., and Marano, F. (1993) Effect of mineral particles containing iron on primary

cultures of rabbit tracheal epithelial cells: possible implication of oxidative stress. *Environ Health Perspect* 101, 436-442.

(23) Guilianelli, C., Baeza-Squiban, A., Lapait, E., and Marano, F. (1996) Cultured airway epithelium responses to mineral particles: role of the oxidative stress. *Toxicology Letters* 88, 39-44.

(24) Lay, J. C., Bennett, W. D., Ghio, A. J., Bromberg, P. A., Costa, D. L., Kim, C. S., Koren, H. S., and Devlin, R. B. (1999) Cellular and biochemical response of the human lung after intrapulmonary instillation of ferric oxide particles. *Am. J. Respir. Cell Mol. Biol.* 20, 631-642.

(25) Fubini, B., Fenoglio, I., and Tomatis, M. (2007) Physico-chemical characteristics of nanoparticles which determine their potential toxicity. In *Nanotoxicology: Characterization, Dosing and Health Effects on Target Organs* pp 59-70, Monteiro-Riviere N. and Tran Lang C. . Informa Healthcare.

(26) Fubini, B., Ghiazza, M., and Fenoglio, I. (2010) Physico-chemical features of engineered nanoparticles relevant to their toxicity. *Nanotoxicology* 4, 347-363.

(27) Nel, A., Xia, T., Madler, L., and Li, N. (2006) Toxic potential of materials at the nanolevel. *Science* 311, 622-627.

(28) Zhu, M. T., Feng, W. Y., Wang, B., Wang, T. C., Gu, Y. Q., Wang, M., Wang, Y., Ouyang, H., Zhao, Y. L., and Chai, Z. F. (2008) Comparative study of pulmonary responses to nano- and submicron-sized ferric oxide in rats. *Toxicology* 247, 102-111.

(29) Wang, B., Feng, W. Y., Zhu, M. T., Wang, Y., Wang, M., Gu, Y. Q., Ouyang, H., Wang, H. J., Li, M., Zhao, Y. L., Chai, Z. F., and Wang, H. F. (2009) Neurotoxicity of low-dose repeatedly

intranasal instillation of nano- and submicron-sized ferric oxide particles in mice. *Journal of Nanoparticle Research* 11, 41-53.

(30) Karlsson, H. L., Gustafsson, J., Cronholm, P., and Moller, L. (2009) Size-dependent toxicity of metal oxide particles--a comparison between nano- and micrometer size. *Toxicol Lett* 188, 112-118.

(31) Radu, M., Munteanu, M. C., Petrache, S., Serban, A. I., Dinu, D., Hermenean, A., Sima, C., and Dinischiotu, A. (2010) Depletion of intracellular glutathione and increased lipid peroxidation mediate cytotoxicity of hematite nanoparticles in MRC-5 cells. *Acta Biochim. Pol.* 57, 355-360.

(32) Bhattacharya, K., Davoren, M., Boertz, J., Schins, R. P., Hoffmann, E., and Dopp, E. (2009) Titanium dioxide nanoparticles induce oxidative stress and DNA-adduct formation but not DNA-breakage in human lung cells. *Part Fibre Toxicol* 6, 17.

(33) Zhu, M. T., Wang, B., Wang, Y., Yuan, L., Wang, H. J., Wang, M., Ouyang, H., Chai, Z. F., Feng, W. Y., and Zhao, Y. L. (2011) Endothelial dysfunction and inflammation induced by iron oxide nanoparticle exposure: Risk factors for early atherosclerosis. *Toxicol Lett* 203, 162-171.

(34) Fubini, B., Aust, A. E., Bolton, R. E., Borm, P. J., Brunch, J., Ciapetto, G., Donaldson, K., Elias, Z., Gold, J., Jaurand, M. C., Kane, A. B., Lison, D., and Muhle, J. (1998) Non animal tests for evaluating the toxicity of solid xenobiotics. pp 579-617, ATLAS, Nottingham.

(35) Sugimoto, T., Wang, Y. S., Itoh, H., and Muramatsu, A. (1998) Systematic control of size, shape and internal structure of monodisperse alpha-Fe₂O₃ particles. *Colloids and Surfaces A-Physicochemical and Engineering Aspects* 134, 265-279.

- (36) Tomatis, M., Turci, F., Ceschino, R., Riganti, C., Gazzano, E., Martra, G., Ghigo, D., and Fubini, B. (2010) High aspect ratio materials: role of surface chemistry vs. length in the historical "long and short amosite asbestos fibers". *Inhalation Toxicology* 22, 984-998.
- (37) Polimeni, M., Gazzano, E., Ghiazza, M., Fenoglio, I., Bosia, A., Fubini, B., and Ghigo, D. (2008) Quartz inhibits glucose 6-phosphate dehydrogenase in murine alveolar macrophages. *Chem Res Toxicol* 21, 888-894.
- (38) Ghigo, D., Aldieri, E., Todde, R., Costamagna, C., Garbarino, G., Pescarmona, G., and Bosia, A. (1998) Chloroquine stimulates nitric oxide synthesis in murine, porcine, and human endothelial cells. *J. Clin. Invest* 102, 595-605.
- (39) Singh, N. P., McCoy, M. T., Tice, R. R., and Schneider, E. L. (1988) A simple technique for quantitation of low-levels of DNA damage in individual cells. *Experimental Cell Research* 175, 184-191.
- (40) Chernyshova, I. V., Hochella, M. F., and Madden, A. S. (2007) Size-dependent structural transformations of hematite nanoparticles. 1. Phase transition. *Physical Chemistry Chemical Physics* 9, 1736-1750.
- (41) Wang, J. W., and Rustad, J. R. (2006) A simple model for the effect of hydration on the distribution of ferrous iron at reduced hematite (012) surfaces. *Geochimica et Cosmochimica Acta* 70, 5285-5292.
- (42) Fubini, B., and Mollo, L. (1995) Role of iron in the reactivity of mineral fibers. *Toxicol Lett* 82-83, 951-960.

- (43) Fenoglio, I., Prandi, L., Tomatis, M., and Fubini, B. (2001) Free radical generation in the toxicity of inhaled mineral particles: the role of iron speciation at the surface of asbestos and silica. *Redox. Rep.* 6, 235-241.
- (44) Hardy, J. A., and Aust, A. E. (1995) Iron in asbestos chemistry and carcinogenicity. *Chem. Rev.* 95, 97-111.
- (45) Aust, A. E., Ball, J. C., Hu, A. A., Lighty, J. S., Smith, K. R., Straccia, A. M., Veranth, J. M., and Young, W. C. (2002) Particle characteristics responsible for effects on human lung epithelial cells. *Res Rep. Health Eff. Inst.*, 1-65.
- (46) Brunner, T. J., Wick, P., Manser, P., Spohn, P., Grass, R. N., Limbach, L. K., Bruinink, A., and Stark, W. J. (2006) In vitro cytotoxicity of oxide nanoparticles: comparison to asbestos, silica, and the effect of particle solubility. *Environ. Sci. Technol.* 40, 4374-4381.
- (47) Voinov, M. A., Sosa Pagan, J. O., Morrison, E., Smirnova, T. I., and Smirnov, A. I. (2011) Surface-mediated production of hydroxyl radicals as a mechanism of iron oxide nanoparticle biotoxicity. *J Am Chem Soc* 133, 35-41.
- (48) Zhu, M. T., Wang, Y., Feng, W. Y., Wang, B., Wang, M., Ouyang, H., and Chai, Z. F. (2010) Oxidative stress and apoptosis induced by iron oxide nanoparticles in cultured human umbilical endothelial cells. *J Nanosci Nanotechnol* 10, 8584-8590.
- (49) Amirbahman, A., Sigg, L., and Gunten, U. (1997) Reductive Dissolution of Fe(III) (Hydr)oxides by Cysteine: Kinetics and Mechanism. *J Colloid Interface Sci* 194, 194-206.

- (50) Tomatis, M., Prandi, L., Bodoardo, S., and Fubini, B. (2002) Loss of surface reactivity upon heating amphibole asbestos. *Langmuir* 18, 4345-4350.
- (51) Kraemer, S. M. (2004) Iron oxide dissolution and solubility in the presence of siderophores. *Aquatic Sciences* 66, 3-18.
- (52) Moller, P., Jacobsen, N. R., Folkmann, J. K., Danielsen, P. H., Mikkelsen, L., Hemmingsen, J. G., Vesterdal, L. K., Forchhammer, L., Wallin, H., and Loft, S. (2010) Role of oxidative damage in toxicity of particulates. *Free Radic Res* 44, 1-46.
- (53) Perez-Benito, J. F. (2004) Iron(III)-Hydrogen peroxide reaction: Kinetic evidence of a hydroxyl-mediated chain mechanism. *Journal of Physical Chemistry A* 108, 4853-4858.
- (54) Zielinski, H., Mudway, I. S., Berube, K. A., Murphy, S., Richards, R., and Kelly, F. J. (1999) Modeling the interactions of particulates with epithelial lining fluid antioxidants. *Am J Physiol* 277, L719-L726.
- (55) Mudway, I. S., Stenfors, N., Duggan, S. T., Roxborough, H., Zielinski, H., Marklund, S. L., Blomberg, A., Frew, A. J., Sandstrom, T., and Kelly, F. J. (2004) An in vitro and in vivo investigation of the effects of diesel exhaust on human airway lining fluid antioxidants. *Arch Biochem Biophys* 423, 200-212.
- (56) Brown, D. M., Beswick, P. H., Bell, K. S., and Donaldson, K. (2000) Depletion of glutathione and ascorbate in lung lining fluid by respirable fibres. *Ann Occup Hyg* 44, 101-108.

- (57) Fenoglio, I., Fonsato, S., and Fubini, B. (2003) Reaction of cysteine and glutathione (GSH) at the freshly fractured quartz surface: a possible role in silica-related diseases? *Free Radic Biol Med* 35, 752-762.
- (58) Wink, D. A., and Mitchell, J. B. (1998) Chemical biology of nitric oxide: Insights into regulatory, cytotoxic, and cytoprotective mechanisms of nitric oxide. *Free Radic Biol Med* 25, 434-456.
- (59) Garcon, G., Gosset, P., Maunit, B., Zerimech, F., Creusy, C., Muller, J. F., and Shirali, P. (2004) Influence of iron ($^{56}\text{Fe}_2\text{O}_3$ or $^{54}\text{Fe}_2\text{O}_3$) in the upregulation of cytochrome P4501A1 by benzo[a]pyrene in the respiratory tract of Sprague-Dawley rats. *J. Appl. Toxicol.* 24, 249-256.
- (60) Aldieri, E., Ghigo, D., Tomatis, M., Prandi, L., Fenoglio, I., Costamagna, C., Pescarmona, G., Bosia, A., and Fubini, B. (2001) Iron inhibits the nitric oxide synthesis elicited by asbestos in murine macrophages. *Free Radic. Biol. Med.* 31, 412-417.
- (61) Park, S. H., and Aust, A. E. (1998) Regulation of nitric oxide synthase induction by iron and glutathione in asbestos-treated human lung epithelial cells. *Arch. Biochem. Biophys.* 360, 47-52.
- (62) Becher, R., Bucht, A., +yvrevik, J., Hongslo, J. K., hlman, H. J., muelsen, J. T., and hwarze, P. E. (2007) Involvement of NADPH Oxidase and iNOS in Rodent Pulmonary Cytokine Responses to Urban Air and Mineral Particles. *Inhalation Toxicology* 19, 645-655.
- (63) Ghiazza, M., Polimeni, M., Fenoglio, I., Gazzano, E., Ghigo, D., and Fubini, B. (2010) Does vitreous silica contradict the toxicity of the crystalline silica paradigm? *Chem Res Toxicol* 23, 620-629.

- (64) Yan, H., and Zhang, B. (2011) In vitro cytotoxicity of monodispersed hematite nanoparticles on Hek 293 cells. *Material Letters* 65, 815-817.
- (65) Wottrich, R., Diabate, S., and Krug, H. F. (2004) Biological effects of ultrafine model particles in human macrophages and epithelial cells in mono- and co-culture. *International Journal of Hygiene and Environmental Health* 207, 353-361.
- (66) Karlsson, H. L., Cronholm, P., Gustafsson, J., and Moller, L. (2008) Copper oxide nanoparticles are highly toxic: A comparison between metal oxide nanoparticles and carbon nanotubes. *Chem Res Toxicol* 21, 1726-1732.

FIGURE LEGENDS

Figure 1. Powder XRD patterns of samples: Hem_nano (a); Hem_submicro (b); Hem_micro (c) showing only the peaks due to hematite (α -Fe₂O₃).

Figure 2. FE-SEM pictures of samples: Hem_nano (a); Hem_submicro (b) and Hem_micro (c).

Figure 3. TEM pictures of Hem_nano (a); Hem_submicro (b); Hem_micro (c and d). Inset to section c) reports SAED patterns.

Figure 4. Particles Size Distribution (PSD) of samples Hem_nano (a), Hem_submicro (b) and Hem_micro (c) suspended in RPMI.

Figure 5. Micro-Raman spectra, in the 150-1800 cm⁻¹ range of samples: Hem_micro (1), Hem_submicro (2) and Hem_nano (3). The inset shows a curve-fitting of Hem_nano spectrum in the 530-740 cm⁻¹ range.

Figure 6. Fe⁺² ions mobilization reported as amount of Fe²⁺ ions released *per* unit surface ($\mu\text{mol m}^{-2}$) as a function of time, upon incubation with ferrozine: Hem_micro (diamonds), Hem_submicro (circles) and Hem_nano (squares). A first order reaction ($y = y_p - Ae^{-kt}$) has been used to fit the data.

Figure 7. Bioavailable iron reported as amount of iron ions released *per* unit surface ($\mu\text{mol m}^{-2}$), upon incubation with ferrozine and ascorbic acid, as a function of time: Hem_micro (diamonds), Hem_submicro (circles) and Hem_nano (squares). A first order reaction ($y = y_p - Ae^{-kt}$) has been used to fit the data.

Figure 8. Effect of hematite particles on LDH release into the extracellular medium of MH-S cells. Cells were incubated for 24 h in the absence (0) or presence of 20-40-80-100 $\mu\text{g cm}^{-2}$ of Hem_nano, Hem_submicro, Hem_micro particles or positive control. Measurements were performed in duplicate, and data are presented as means \pm SEM (n = 3). Vs ctrl * p<0.0001.

Figure 9. Induction of apoptosis/necrosis by hematite particles in MH-S cells. Cells were incubated for 24 h in the absence (0) or presence of 20-40-80-100 $\mu\text{g cm}^{-2}$ of Hem_nano, Hem_submicro, Hem_micro particles or positive control. After incubation, the fluorescence of cell-associated annexin V-FITC (panel A) and PI (panel B) was measured. Results are expressed as a percentage increase of fluorescence versus the respective control incubated without particles (assumed a 100%). Measurements were performed in duplicate, and data are presented as means \pm SEM (n = 3). Panel A: vs ctrl * p<0.05, ** p<0.0001 Panel B: vs ctrl * p<0.05, ** p<0.0001.

Figure 10. Effect of hematite particles on DNA damage (measured as % tail DNA) in MH-S cells. Cells were incubated for 24 h in the absence (0) or presence of 40 $\mu\text{g cm}^{-2}$ of Hem_nano, Hem_submicro, Hem_micro particles or 20 $\mu\text{g cm}^{-2}$ of positive control. Data are presented as means \pm SEM. (n = 3). At least 50 cells were evaluated in each experiment. Vs ctrl * p<0.0001.

Figure 11. Effect of hematite particles on extracellular levels of nitrite in MH-S cells. Cells were incubated for 24 h in the absence (0) or presence of 20-40-80-100 $\mu\text{g cm}^{-2}$ of Hem_nano, Hem_submicro, Hem_micro particles or positive control. After incubation, nitrite accumulation in the culture supernatant was determined as described in the Materials and Methods section.

Measurements were performed in duplicate, and data are presented as means \pm SEM. (n = 3). Vs ctrl * p<0.0001.

Table 1. Average particles diameter (nm) and specific surface area ($\text{m}^2 \text{g}^{-1}$) of the studied samples. Last column: average crystallites size (nm) as derived by applying the Scherrer equation to powder XRD patterns.

Sample	Particles diameter from FE-SEM (nm)^a	Particles diameter from TEM (nm)^a	Measured SSA ($\text{m}^2 \text{g}^{-1}$)^b	Calculated SSA ($\text{m}^2 \text{g}^{-1}$)^c	Crystallites size (nm)^d
Hem_nano	87 (11)	93 (8)	19-22	14	88
Hem_submicro	238 (65)	260 (32)	4-8	5	256
Hem_micro	1100 (200)	1600 (460)	13-14	0.7	52

^a Average particles diameter, as obtained by analyzing either FE-SEM or TEM micrographs by means of the Image J software; standard deviation values reported in round brackets. .

^b SSA as obtained by applying the Brunauer-Emmett-Teller (BET) algorithm to N_2 isotherms at -196°C ; .

^c SSA as calculated on geometrical basis by using the average particles diameters obtained by FE-SEM analysis. .

^d Average crystallites size, obtained by at least three XRD spectra for each sample.

Table 2. Particle hydrodynamic diameter (PHD); Poly-Dispersion Index (PDI) and average dimensions as obtained by DLS measurements of powders dispersed in biologic medium (RMIP suspension). Standard deviation values reported in round brackets.

Sample	Particle diameter from PSDs (Mean, nm)				PDI
	PHD ^a	Intensity ^b	Number ^b	Volume ^b	
Hem_nano	68 (3)	79 (11)	45 (3)	69 (22)	0.146
Hem_submicro	190 (7)	252 (13)	96 (7)	357 (27)	0.285
Hem_micro	762 (94)	821 (100)	740 (58)	888 (125)	0.392

^a Particle hydrodynamic diameter, which represents the apparent size of solvated particles;

^b Values calculated in the 2-3000 nm range.

Table 3 Depletion of antioxidant defences: amount of cysteine consumed per unit surface ($\mu\text{mol m}^{-2}$) after 30 and 180 minutes of incubation in a 0.1 mM solution of cysteine in phosphate buffer.

Sample	Amount of cysteine consumed ($\mu\text{mol m}^{-2}$)	
	after 30 min	after 18 min
Hem_micro	0.01 ± 0.002	0.5 ± 0.06
Hem_submicro	0.01 ± 0.001	0.4 ± 0.05
Hem_nano	0.01 ± 0.002	0.3 ± 0.05

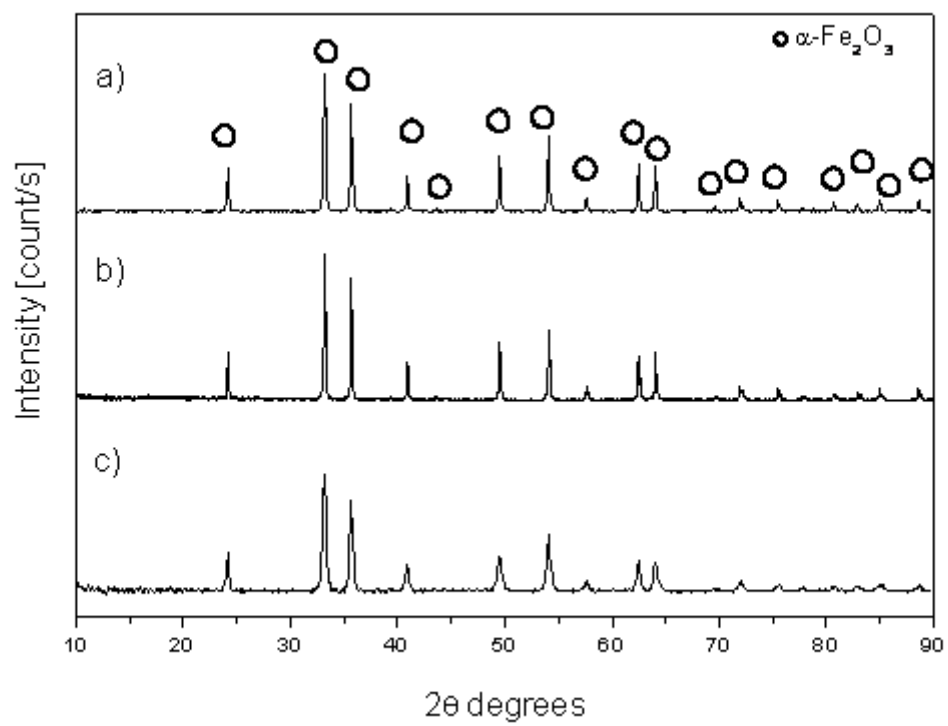


Figure 1. F.S. Freyria et al.

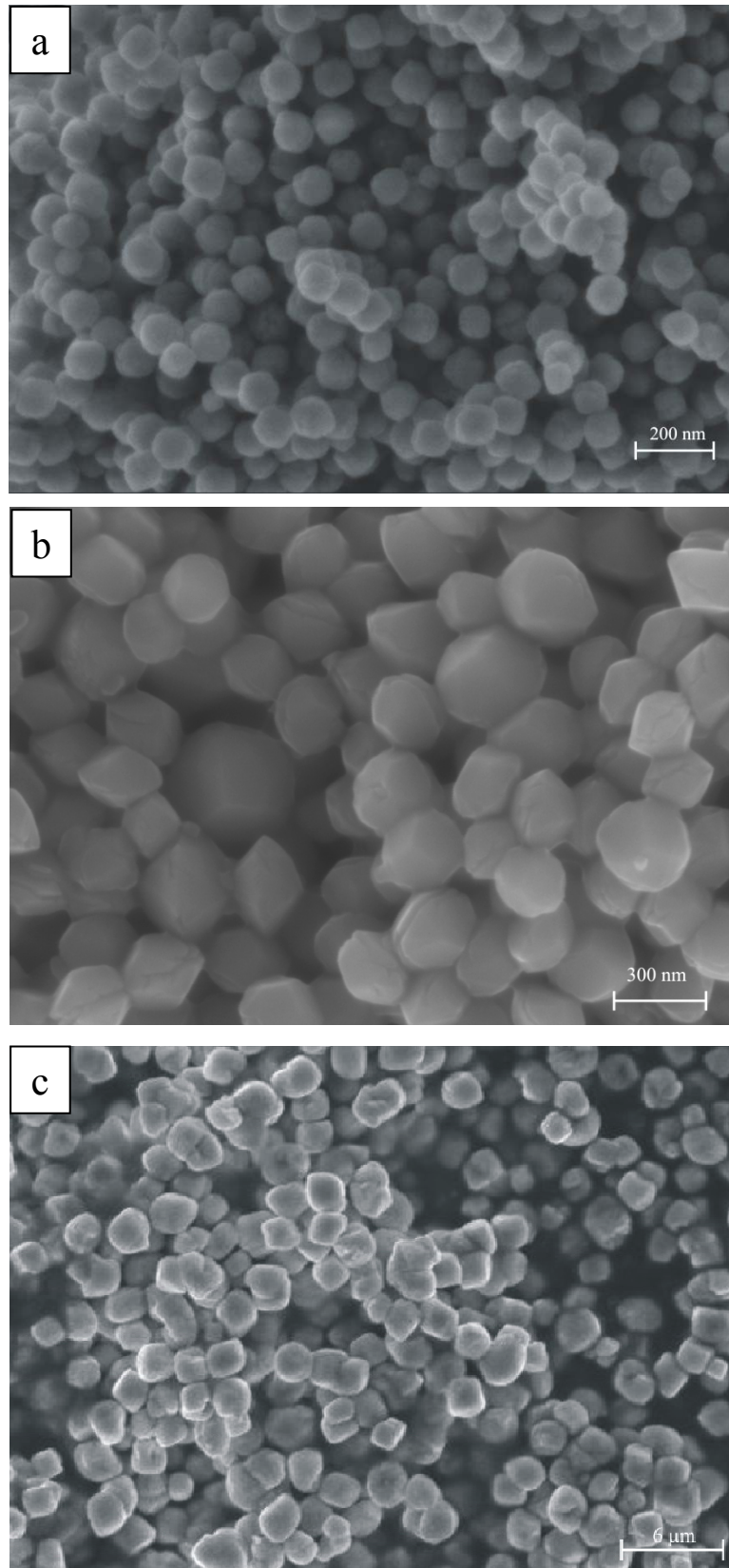


Figure 2. F.S. Freyria et al.

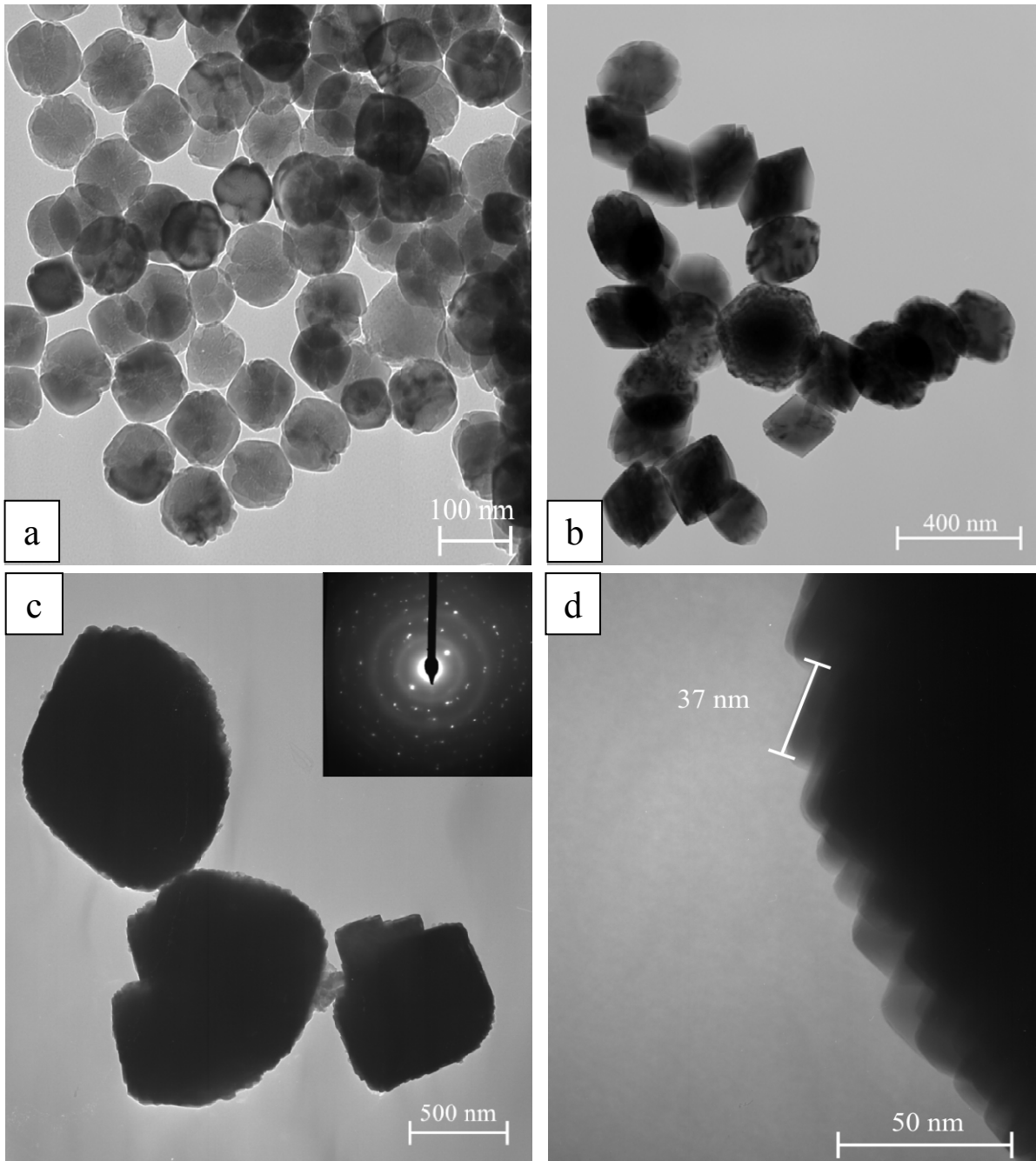


Figure 3. F.S. Freyria et al.

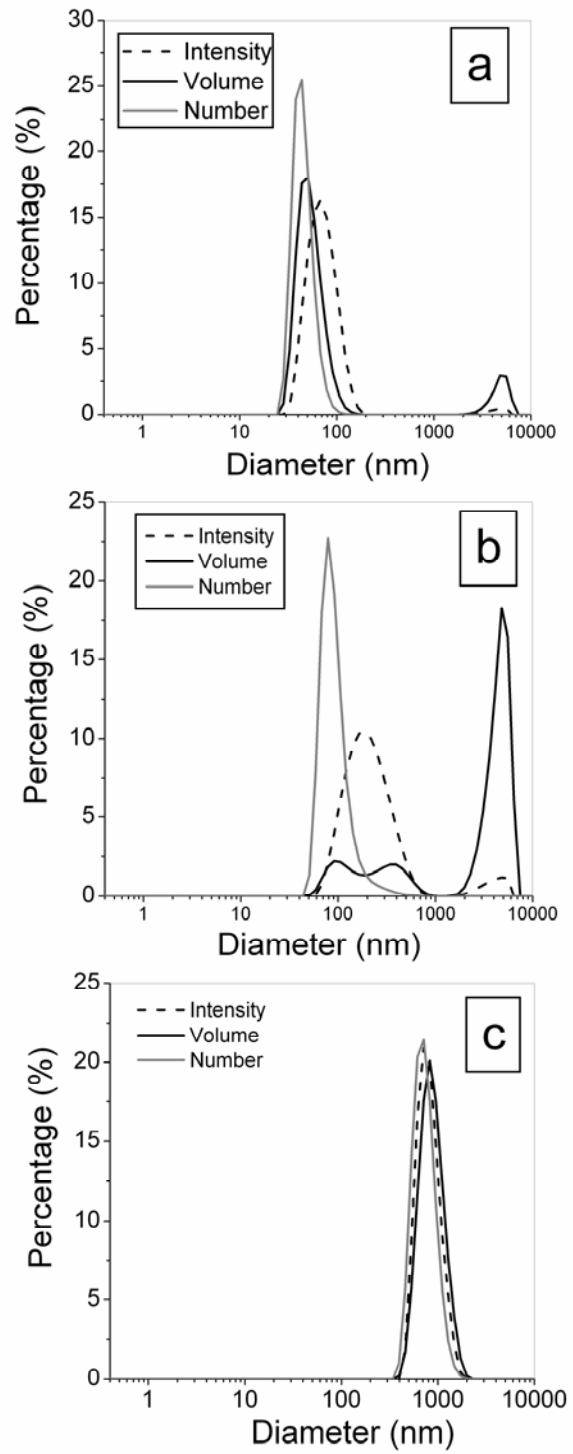


Figure 4. F.S. Freyria et al.

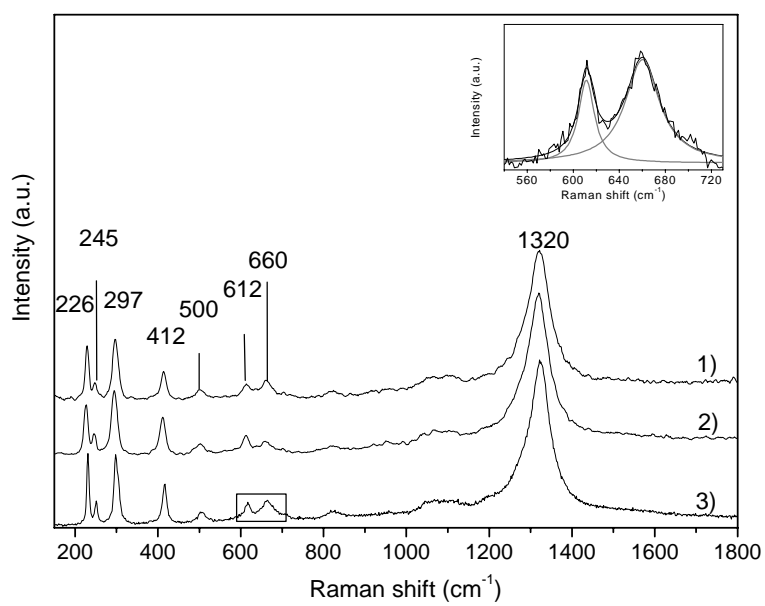


Figure 5. F.S. Freyria et al.

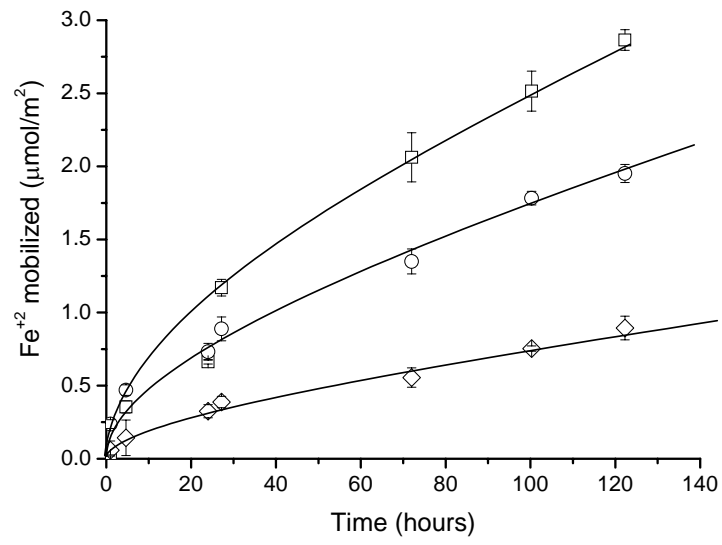


Figure 6. F.S. Freyria et al.

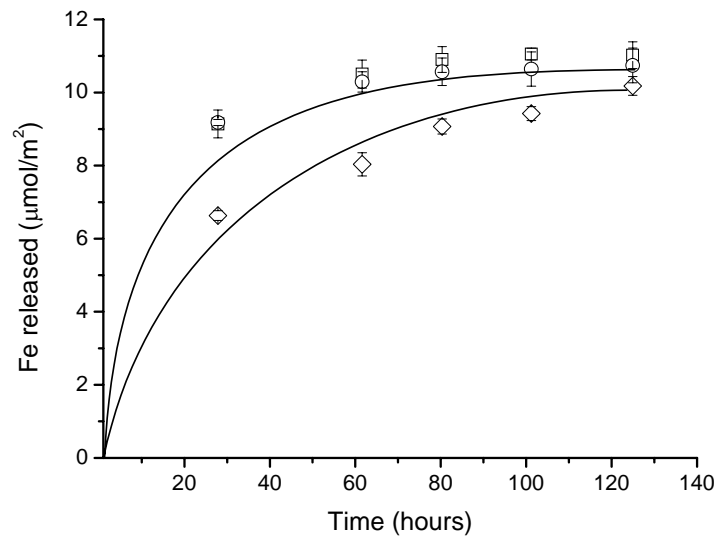


Figure 7. F.S. Freyria et al.

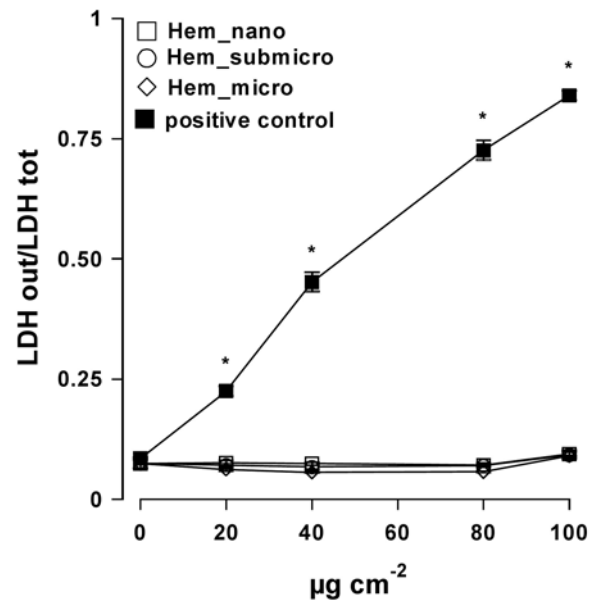


Figure 8. F.S. Freyria et al.

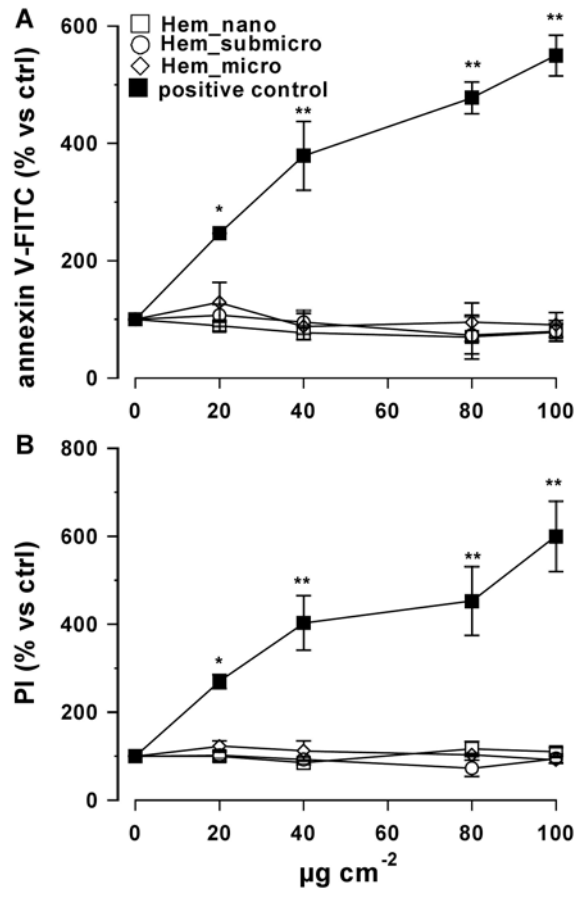


Figure 9. F.S. Freyria et al.

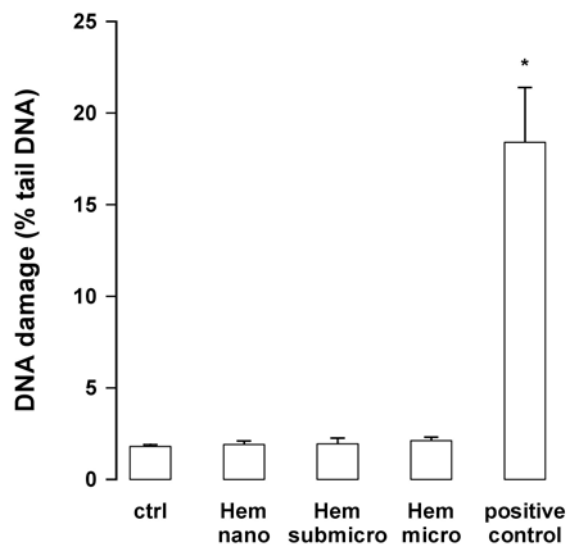


Figure 10. F.S. Freyria et al.

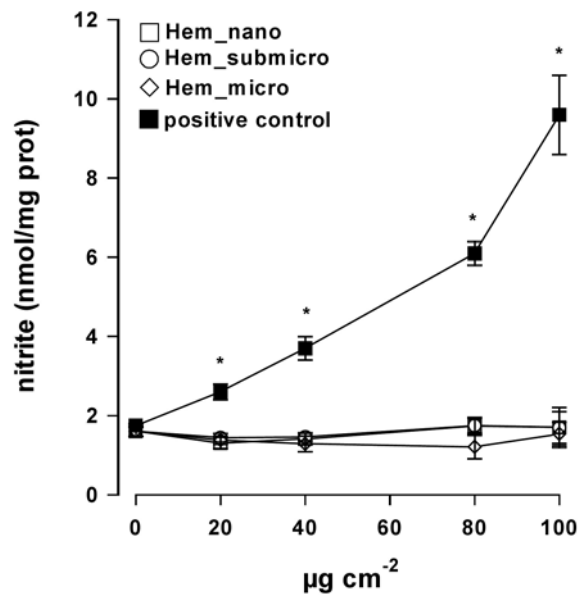


Figure 11. F.S. Freyria et al.